ADVANCED OPTICAL MATERIALS
www.advopticalmat.de

Metal–Semiconductor–Metal Metasurface for Multiband Infrared Stealth Technology Using Camouflage Color Pattern in Visible Range

*Jagyeong Kim, Changhoon Park, and Jae W. Hahn**

Optical stealth technology is being developed to cope with high-sensitivity infrared image detectors and various guided detectors. Infrared stealth technology has remarkable performance; however, future advancements in multi-band stealth technology covering the entire optical frequency range, from visible to wide infrared, are key challenges regarding unmanned surveillance systems. Thus, a metal–semiconductor–metal (MSM) metasurface with Fabry–Pérot (F–P) and multiple plasmonic resonant modes is introduced to realize multiband stealth technology. Different colors are obtained for printing camouflage patterns in the visible range using localized surface plasmon modes in Al disks on an opaque Ge layer. The F–P resonance of the Ge layer induces a strong absorption of >92% at 1.06 μm, reducing the guidance signal of the infrared laser-guided detector. With an additional plasmonic resonance in the MSM metasurface, infrared signature reductions of >34%, >94.4%, and >97.7% are obtained for short-wave, mid-wave, and long-wave infrared bands, respectively.

1. Introduction

Camouflage refers to the ability of certain animals to blend with their surroundings in the visible range using an adaptable multicolor pattern, which is indispensable for their survival rate against predators.[1–6] With advancements in infrared (IR) technology,[7–15] various high-sensitive detectors with wide IR spectral ranges have been developed and popularized in military and surveillance applications.[16] Owing to the low observability against IR detectors, IR stealth technology has also been extended to the wide IR spectral range.[17–20] An IR signature is determined by the magnitude of a signal obtained by IR detectors that measure the thermal radiation from an object; IR stealth technology reduces this IR signature.[7,11–12] As the thermal radiation from an object is weak, most IR image detectors in the near IR (NIR: 0.75–1.4 μm) and shortwave IR (SWIR: 1.4–3.0 μm) ranges measure reflected signals from objects in the conventional operational temperature range of military equipment.[16] Therefore, to achieve low observability over a wide spectral range from NIR to LWIR, the surface of an object must simultaneously suppress the reflected light in the NIR and SWIR ranges as well as the thermal radiation in the mid-wave IR (MWIR: 3–8 μm) and longwave IR (LWIR: 8–14 μm) ranges.

IR stealth technology has been developed considerably; however, future advancements in multiband stealth technology covering the entire optical frequency range, from the visible to the wide IR range, are key challenges faced by unmanned surveillance systems.[17–21] To address the low observability in the MWIR and LWIR ranges, various types of frequency-selective devices have been proposed based on the concept of a plasmonic metasurface that controls the tunability of spectral characteristics to avoid the detectable range of IR detectors.[7–8,11–12,19] Metal–insulator–metal (MIM) nanostructures have been widely employed in multispectral engineering[22–27] with the excitation of surface plasmon polaritons[28–29] and magnetic polaritons.[30–32] Studies on the extending the application of optical stealth technology in the multi-infrared band have been actively conducted using various optical device concepts.[17,18,20] Regardless of camouflage pattern printing, structural color filters with subwavelength nanostructures have been extensively studied to excite either photonic or plasmonic resonant modes.[33–41]

Although pioneering studies[11,17,20] on dielectric multilayer structures have been recently conducted to achieve broadband performance, their application remains limited owing to the difficulties in realizing high narrowband absorption performance for guided laser and visible camouflage pattern printing. Herein, we propose a new platform for an optical stealth material with an MSM structure-based metasurface for suppressing scattered light in the NIR and SWIR ranges as well as emitted thermal radiation in the MWIR and LWIR ranges. We adjusted the design parameters to activate multiple resonances independently with a small interference in the wide spectral band. To

J. Kim, C. Park, J. W. Hahn
Nano Photonics Laboratory
School of Mechanical Engineering
Yonsei University
50 Yonsei-ro, Seodaemun-gu, Seoul 120–749, Republic of Korea
E-mail: jaewhahn@yonsei.ac.kr

The ORCID identification number(s) for the author(s) of this article can be found under https://doi.org/10.1002/adom.202101930.

DOI: 10.1002/adom.202101930

address the practical usability of the proposed metasurface, we demonstrate camouflage color patterns and analyze the performance of the metasurface in terms of potential for application in IR stealth technology.

2. Concept of Multiband IR Stealth Technology with Camouflage Color Patterns

To deceive the human eye or a visible-range camera with a camouflage pattern, chromatic color generation with subwavelength-scale pixel size is required to assimilate the surface of an object to the external environment.[6] For multiband IR stealth technology, the following functionalities are required: 1) high absorptivity in NIR and SWIR for deception of laser tracking system, SWIR camera, and night vision goggles; 2) low thermal radiation in the MWIR and LWIR ranges. In the NIR and SWIR ranges, wherein night vision goggles, SWIR cameras, and laser tracking systems are used to detect an object, the reflective signature of the surface should be suppressed so that the detection system cannot capture the military object. Meanwhile, for the thermal detection in the MWIR and LWIR ranges, a low emissive surface is required to suppress the thermal radiation signal from the high-temperature military unit.

Gap plasmon metasurfaces with MIM geometry have been extensively employed due to their resonance tunability and high-frequency selectivity performance based on localized surface plasmon resonance (LSPR) and surface lattice resonance.[22–24,30–32] If only gap plasmon or lattice coupling is considered, MIM metasurfaces have a restricted spectral range, only allowing a limited number of resonance modes. However, by employing semiconductor bandgap materials between the metal layers, which are transparent in the IR range and opaque in the visible range, the number of resonance modes in MSM metasurfaces can be increased. We adopted an MSM structure to realize multispectral selective engineering. **Figure 1** illustrates an MSM metasurface consisting of a disk resonator. This configuration can help extend the spectral range of a metasurface significantly, which is beneficial to multispectral engineering.

A Ge layer functions as a highly absorbing medium[34,42,43] in the visible and NIR ranges, suppressing light transmission inside the Ge layer. Owing to the short skin depth of the Ge layer, most of the light energy cannot be delivered to the bottom metal layer, and Ge/Ag becomes a reflective substrate. However, contrary to the lossless dielectric property in the wide IR range, the high conductivity of the Ge layer strongly affects the optical response of Ge/Ag multilayers in the visible and NIR ranges. The high imaginary value of the refractive index in a Ge layer leads to nontrivial reflection phase shifts at the Ge and Ag interfaces, resulting in a destructive interference condition even for an ultrathin optical path length. Thus, Ge/Ag multilayers exhibit frequency-selective reflectivity with neglection of the upper metallic structure. While blocking thermal radiation energy in the MWIR and LWIR ranges with low emissivity, MSM metasurfaces exhibit high absorptivity in the NIR and SWIR ranges. Furthermore, engineered spectral absorptivity for visible wavelengths enables MSM metasurfaces to exhibit full color with a sub-wavelength pixel size. Contrary to conventional gap plasmon metasurfaces with highly reflective substrates, the multispectral selective performance of MSM metasurfaces originates from a frequency-selective substrate constituting a semiconductor/metal layer.

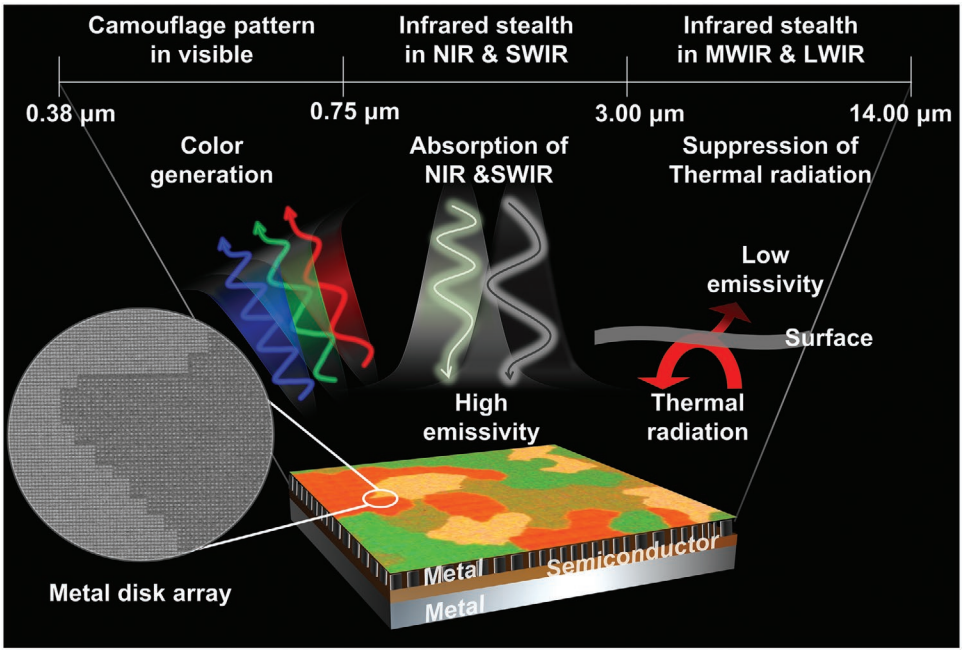

Figure 1. Camouflage patterns of MSM structure in visible and wide-band IR stealth. For visible wavelengths, a camouflage pattern comprising an MSM structure with various colors deceives the human eye or a visible-range camera. To achieve low observability against reflection-type IR detection systems, the MSM structure exhibits high absorptivity in the NIR and SWIR ranges. For thermal camouflage applied to a high-temperature system, the MSM structure suppresses the thermal signature in the MWIR and LWIR ranges.

As the Ge semiconductor layer becomes opaque in the visible and NIR ranges, the LSPR can be excited in the periodic metal disk pattern on the semiconductor layer without accounting for the entire MSM structure. Thus, we propose a metasurface with a periodic nanoscale metal disk pattern on a Ge semiconductor layer to realize color pixels. With engineered reflectivity in the visible spectrum, the metasurface exhibits chromatic color with a sub-wavelength-scale pixel size. For the calculations in **Figure 2**, a 35-nm-thick Ge layer and a 70-nm-thick Al pattern with the radius varying from 95 to 205 nm in 10 nm steps and a period from 285 to 655 nm were used. Figure 2a illustrates the optical power distribution in the LSPR condition, yielding maximum spectral absorptivity. At the visible frequency, optical energy cannot be delivered to the bottom metallic surface through the Ge[34] layer, and LSPR is mainly activated in the Al[44] disk. In the NIR range, the Ge/Ag[42,45] multilayers cause absorption via the Fabry–Pérot (F–P) destructive interference condition. Figure 2b shows the power distribution under this condition. The destructive interference condition in these systems is determined from the optical path length (OPL), which is $n_{Ge}t_{Ge}$, and the phase shift induced by reflection at the interface of the Ge/Ag layer. Here, n is the refractive index, t is the layer thickness, and the subscript pertains to the material. Contrary to a perfect reflector with a lossless dielectric, the high imaginary value of the refractive index for Ge causes a non-trivial phase shift, leading to the out-of-phase condition with an ultrathin Ge layer (Supporting information 1). In contrast to the NIR range, where the conductivity of Ge[43] is finite, the Ge layer becomes a lossless material in the SWIR range, and a gap plasmon mode in the MSM structure is realized. As illustrated in Figure 2c, optical power is efficiently confined in the Ge layer under the gap plasmon resonance condition. As the gap plasmon resonance wavelength is affected by the lateral dimension of the Al disk pattern as well as the dielectric thickness of the Ge film, a larger Al disk supports plasmonic resonance in a long-wavelength range (Supporting information 2).

By engineering the LSPR condition with varying geometrical dimensions of the Al disk, we demonstrated various colors ranging from red to green and blue. To estimate the color perceived by the human eye, we calculated the tristimulus values based on the reflectivity spectra of the metasurface.[36,37,39,40] Figure 2d presents the color distribution with varying disk radii and fill factors, obtained via the numerical calculation of the reflection spectra. The fill factor is expressed as the ratio of the total area covered by the disk pattern in the Ge film. With an increase in the disk radius, which leads to the redshift of the LSPR wavelength, the estimated color varies from red to blue and green. By suppressing light reflection for short wavelengths, the metasurface comprising a small disk radius reflects light with longer wavelengths, generating green or red color. Meanwhile, the LSPR bandwidth affects the color saturation. For a plasmonic resonator composed of a noble metal and lossless dielectric, a low Ohmic loss yields absorptivity spectra with a sharp bandwidth, and light is reflected, which degrades color saturation. Figure 2e displays the absorptivity spectra of the MSM structure with different Ge thicknesses. Even for nanoscale optical thicknesses, destructive interference is satisfied, and a larger Ge thickness leads to a redshift of the resonance. The resonant peak for a Ge thickness of 35 nm meets the wavelength condition of 1.06 μm for a laser-guided surveillance system. Figure 2f presents the calculated absorptivity spectra of the MSM metasurface in the SWIR range. As the structure exhibiting blue color has a larger radius compared with other colors, gap plasmon resonance is observed in a longer-wavelength region. The excitation plasmon resonance mode can be used to significantly reduce the signature of IR cameras operating in the SWIR range.

In the wavelength range from MWIR to LWIR, the conductivity of the Ge layer is negligible; thus, the Ge medium becomes a lossless dielectric with high transparency. In this range, the Ge/Ag multilayers function as a low-loss reflective substrate without frequency-selective performance and provide high reflectivity at non-resonant frequencies. Figure 2g displays the spectral emissivity of the MSM structure with different radii of the Al pattern matching the red, green, and blue colors in the MWIR and LWIR ranges. The tail of the resonance peak in the MWIR range may contribute slightly to the IR signature by the thermal radiation of high-temperature objects. In the MWIR range, the calculated band emissivity values are 0.02, 0.04, and 0.11 for the red, green, and blue pixels, respectively. Meanwhile, the MSM structure exhibits extremely low band emittance in the LWIR range, smaller than 0.015.

3. Performance Analysis of the MSM Device

We investigated the diversity of color generation on the MSM structure. For low observability from visible surveillance systems, the MSM surface is required to generate a camouflage pattern to blend with the surroundings. Color generation on the MSM structure is mainly influenced by LSPR in the Al disk on the Ge layer as the Ge layer is opaque in the visible range; therefore, the disk radius and fill factor of the disk in the unit cell are the main parameters. To imitate camouflage patterns, we first fabricated a color palette using the MSM structure to determine the range of colors generated and select the colors required for use in the camouflage pattern. **Figure 3**a shows the captured optical microscopy image of color pixels for various radius (95–205 nm) and fill factors (0.22–0.43) of the Al disk pattern. The substrate was prepared with a Ge layer thickness of 35 nm to absorb light at a wavelength of 1.06 μm for low observability against a laser-guided detector.

We demonstrated camouflage color patterns using this MSM device by imitating the certificated camouflage pattern designs of M1999 Belgian and M01 Danish. Based on plasmonic resonance on the semiconductor layer with a metallic pattern, where the colors are exhibited by controlling the fill factor and radius of the circular disk, we printed the camouflage color patterns. To generate the Belgian-type camouflage pattern, which resembles a jigsaw puzzle, as in Figure 3b, we adopted four types of colors with various combinations of the fill factor and disk radius: yellowish green (0.25, 185 nm), green (0.31, 185 nm), reddish brown (0.22, 145 nm), and dark blue (0.28, 165 nm). Meanwhile, the Denmark-type camouflage pattern in Figure 3c shows a yellowish pattern, which was designed for arid areas. To create this pattern, we used three colors; green (fill factor of 0.25, disk radius of 165 nm), brick-red (0.25, 155 nm), and yellow (0.22, 115 nm).

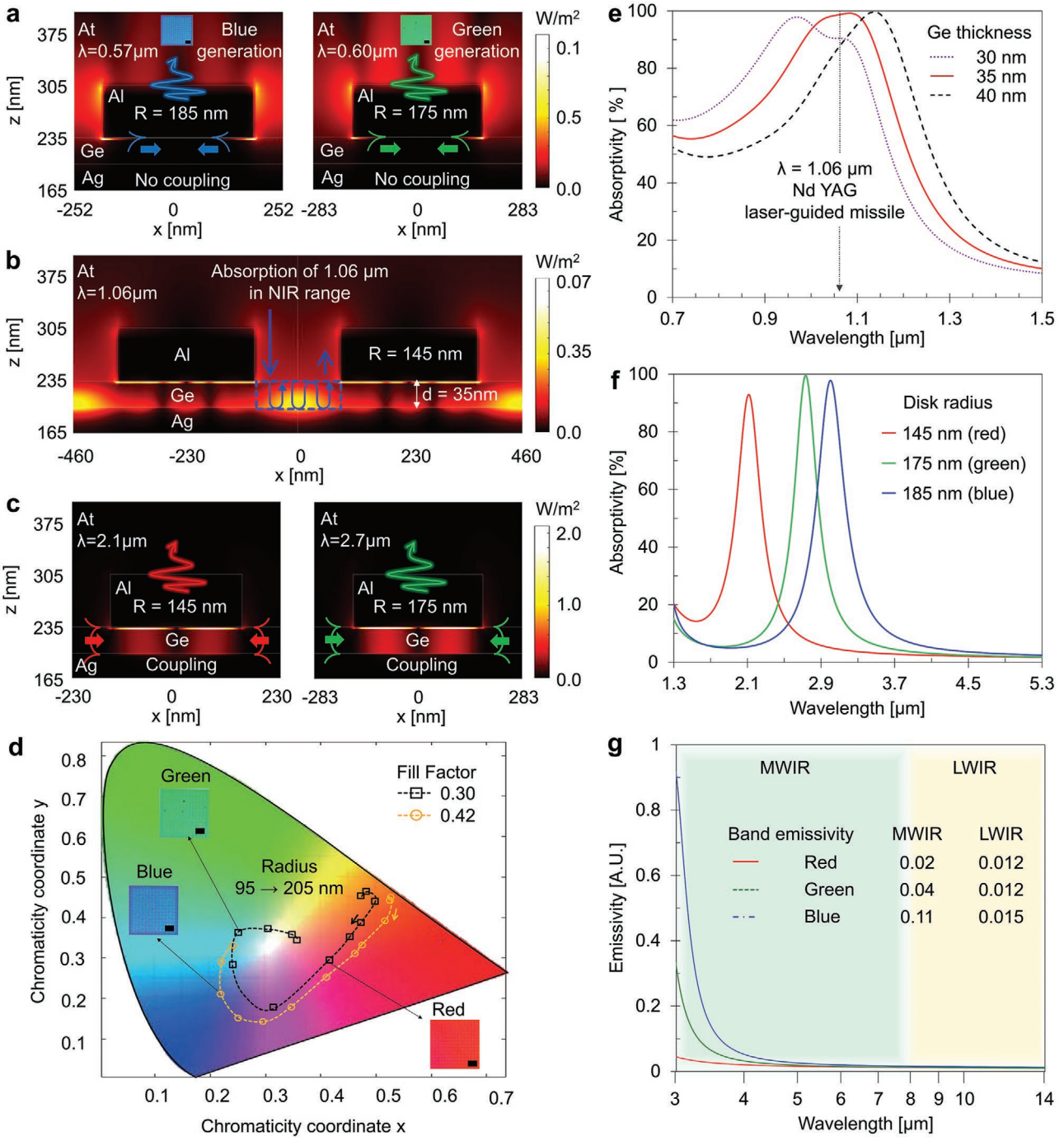

Figure 2. Calculation of multiple resonance modes in MSM metasurface. a) Power distribution of a metasurface for color pixel generation by LSPR mediated with metallic disk, where blue and red colors are generated for disk radii of 185 and 175 nm, respectively. b) Power distribution at destructive Fabry–Pérot interference condition with absorption at the wavelength of the Nd:YAG laser (1.06 μm), where the thickness of the Ge layer is 35 nm. c) Power distribution of gap plasmon resonance in the NIR range. For circular disk radii of 185 and 175 nm, the MSM surface shows high absorption of wavelengths of 3.00 and 2.75 μm, respectively. d) Reflection colors generated by the metasurface in the CIE color spaces. We varied the radius from 95 nm to 205 nm in increments of 10 nm. The two dashed curves with squares and circles represent fill factors of 0.30 (black) and 0.42 (yellow), respectively. e) Absorption spectra of MSM structures in the NIR range calculated for various Ge thicknesses of 30, 35, and 40 nm for an Al disk radius of 145 nm. f)Calculated absorptivity spectra of MSM structure in the SWIR range when the MSM surface generates red, green, and blue colors. g) Calculated emissivity spectra of MSM structures with different colors of red, green, and blue in a, MWIR and b, LWIR ranges. Band emissivity values for various color pixels are indicated.

Figure 3d shows the FTIR spectra of various MSM metasurfaces exhibiting different colors over a wide IR spectral range, from NIR to LWIR. At 1.06 μm, the absorptivity of the MSM metasurface is 92%–96%. The band emissivity values for the

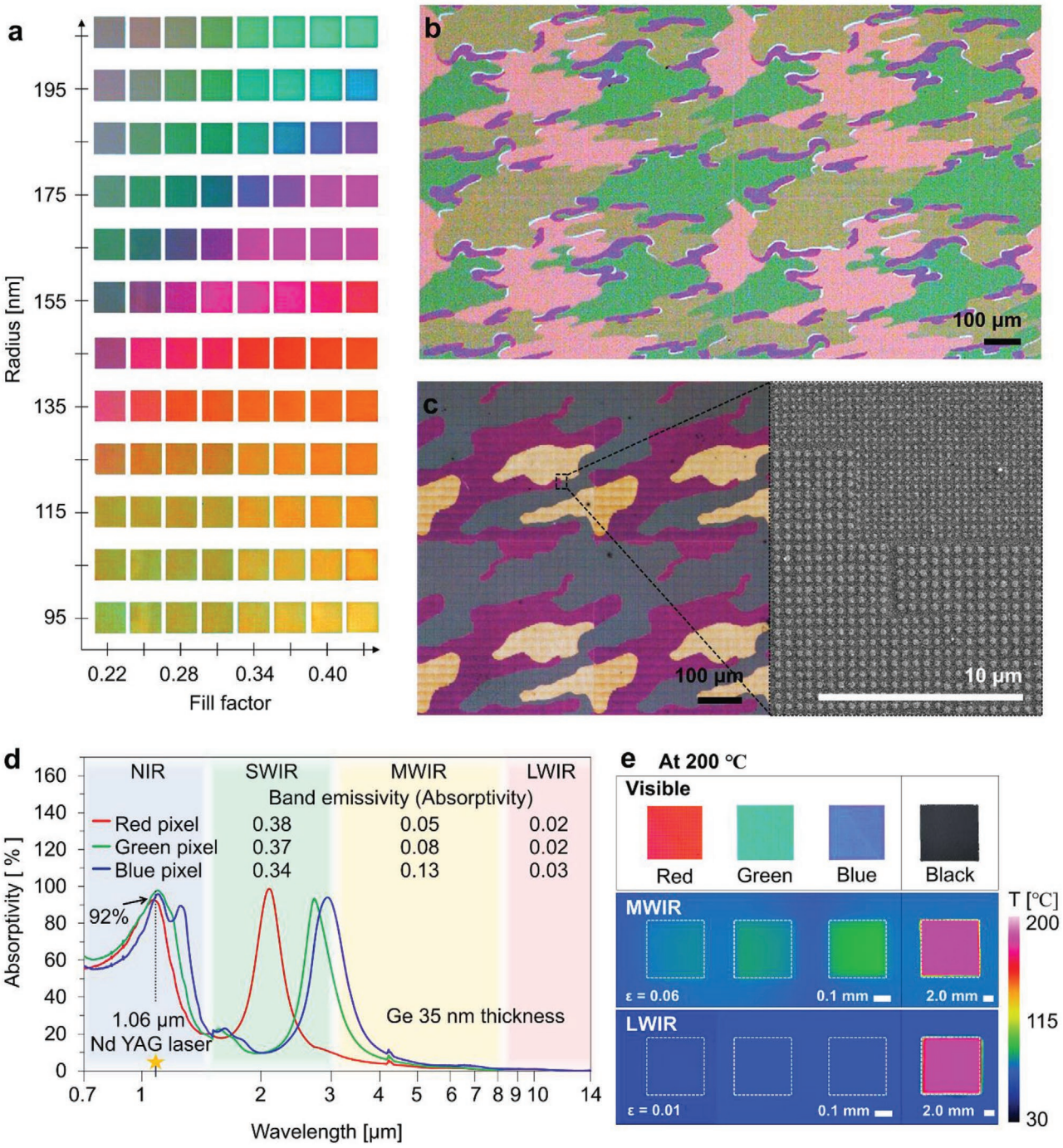

Figure 3. Camouflage patterns printed on the MSM metasurface and FTIR spectrum. a) Optical microscopy image of fabricated color palette. Color palette with different color pixels was generated by varying the disk radius and fill factor of the MSM structure from 95 to 205 nm and from 0.24 to 0.45, respectively. b) Imitation of the Belgian-type pattern (M1999). c) Imitation of the Danish-type pattern (M01) where the inset shows the SEM image of the square dot box area. d) FTIR spectrum of an MSM metasurface with a Ge layer thickness of 35 nm. e) Images captured using the MWIR and LWIR cameras for the various colored cells compared with a black-painted cell at a temperature of 200 °C. *T* represents the apparent temperature.

three color pixels in the wide IR ranges of SWIR, MWIR, and LWIR are listed in the figure. The absorptivity and band emissivity values presented clearly indicate the major stealth performance parameters in a wide IR spectral range. The peak absorptivity at 1.06 μm reduces the laser light signal reflected from the object; thus, laser-guided surveillance systems can be evaded. In the SWIR range, the reduction rate of the IR camera signature by the MSM metasurface ranges from 34% to 38%. Additionally, the reduction rate of MSM metasurfaces of various colors is 82%–97% in the MWIR and LWIR ranges.

To visualize the IR stealth performance of MSM metasurfaces under heating conditions, thermal images of MSM

metasurfaces were compared with those of black-painted surfaces at a temperature of 200 °C in the MWIR and LWIR ranges. The emissivity of the black-painted surface, measured using FTIR spectra, is almost constant over the wide IR range, with an estimated average emissivity of 0.96. The image acquired in the visible range, presented in Figure 3e, shows MSM metasurface cells with dimensions of 300 × 300 μm and a black-painted cell with a size of 1.5 × 1.5 mm. For MWIR, the IR signature reduction compared to the black-painted cell is 94.4%, 90.3%, and 84.8% for the red-, green-, and blue-colored cells, respectively. The reduction rate of the IR signature in the LWIR image is greatly improved, and the cells are rarely recognized by the IR camera. Compared with the cells painted black, the reduction in the IR signature is greater than 97% for all three types of colored cells. The IR signature attenuation obtained in the experiment is less than expected, because the average emissivity in the response IR band of the FLIR detector decreases owing to the spectral response of the detection device (Supporting Information 3).

Further, we quantitatively analyzed the IR stealth performance of the MSM metasurfaces, assuming an ambient temperature of up to 300 °C in a more realistic simulation case. Using the MSM metasurface, we printed a square with the camouflage pattern onto a silver film, as shown in **Figure 4**a. We also printed the same pattern with black paint for comparison. Square images were recorded using MWIR and LWIR cameras while increasing the temperature from 50 to 300 °C. In the left column of Figure 4b, the MWIR images of squares printed with the MSM metasurface are compared with those printed with black paint. Similarly, comparisons of the LWIR images of squares are shown in the right column of the figure. For the MWIR images, the square is barely recognizable at temperatures up to 300 °C, and for the LWIR images, the square is invisible over the entire temperature range tested. The apparent temperatures determined with the MWIR and LWIR cameras are presented in Figure 4c. The apparent temperature of the MSM metasurface is lower than that of the painted black surface in the ranges of 46–146 °C and 15–190 °C for the MWIR and LWIR images, respectively. One of the key specifications of IR stealth technology is the rate of reduction of IR signatures in MWIR and LWIR images. To evaluate the reduced IR signature of the MSM metasurface in comparison with other materials, we normalized the IR signature of the MSM metasurface to that of a blackbody, which is defined as the reduction rate of the IR signature. As shown in Figure 4d, when the reduction rate is calculated using the measured FTIR spectrum, a reduction of more than 94.4% over the temperature range is obtained in the MWIR images, and the reduction decreases slightly with temperature. For LWIR images, the estimated reduction rate exceeds 97.7% and is almost constant over the temperature range.

4. Conclusion

In summary, we proposed a new platform for an optical stealth material using an MSM metasurface with multiple resonant modes to realize stealth technology over a wide spectral range. We successfully demonstrated the ability of MSM structures to extend the potential application of metasurfaces. A color pallet comprising various colors was demonstrated with the MSM metasurface, and camouflage patterns were printed using the realized different colored pixels. In terms of IR stealth technology, an absorption peak of 1.06 μm is greater than 92% and can reduce the reflected laser signal of military targets attacked by an IR laser-guided detector. Moreover, plasmon resonance in the SWIR range can reduce the signal by 34%, degrading the IR images. To cope with MWIR and LWIR imaging guided surveillance systems, the MSM metasurface exhibits low emissivities of less than 0.05 and 0.01 in the MWIR and LWIR wavelength ranges, respectively. We quantitatively evaluated the IR stealth performance based on the reduction in thermal radiation by the MSM metasurface and obtained signature reductions of more than 94.4% and 97.7% for the MWIR and LWIR images over a temperature range up to 300 °C, respectively. The stealth material proposed in this work is robust for real-world applications owing to its passive material platform. We can expect it to be used for a wide range of optical stealth technology applications by extending its spectral range. To further its practical use, research on the fabrication process for large-sized devices needs to be conducted.

5. Experimental Section

Fabrication: There were many patterning techniques for fabricating metasurfaces formed with nanoscale metal patterns.[8,16,18,30–33,36–40,46] The fabrication process for the MSM metasurface is as follows. After cleaning a Si wafer (P-type, orientation: 100, thickness: 525 μm, resistance: 1–30 Ωcm), a 20-nm-thick Cr layer on the wafer was deposited as an adhesion layer using e-beam evaporation (ULTEC, UEE). Ag and Ge layers with thicknesses of 200 and 35 nm, respectively, were subsequently deposited on the Cr layer. The AR-6200.09 e-beam resist was coated on the deposited semiconductor layer via spin coating, ensuring a thickness of 220 nm, (MIDAS, Spin-1200D) and baked the coated resist on a hot plate (Wisd. laboratory instrument, MSH-20D) at 300 °C for 3 min. By using an e-beam lithography system (NBL, NB3), circular disk arrays were exposed on the positive resist, and patterned by the development process. To form the metallic disk on the semiconductor layer, a 70-nm-thick Al layer was deposited on the patterned disk voids via e-beam lithography. The wafer was immersed in an acetone solution with sonication (MUGIGAE(SEONG DONG)) for 10 min in a lift-off process, and the MSM metasurface was finally obtained. The black painted sample was fabricated by using the spray of Krylon Color Master Paint/Primer/Flat/Black.

Measurement of Spectral Property: To obtain the spectral characteristics in the visible to NIR range (380–1400 nm), microspectroscopy (CRAIC, 20/30/PV) was used. The transmittance was zero due to the thick bottom metal layer, whose thickness exceeded the skin depth of the incident light. Thus, its absorptivity was regarded as $A(\lambda) = 1–R(\lambda)$, where A and R describe the absorptivity and reflectivity, respectively. Therefore, to calculate the absorptivity, the reflectance of the MSM metasurface illuminated was measured by a Xenon lamp with a size of 200 × 200 μm. Reflectance was defined as the ratio between the signature reflected by a perfectly reflective sample and the MSM metasurface.

For the spectral emissivity in the SWIR to LWIR range (1.4–14.0 μm), FTIR spectroscopy (Thermo Scientific, Nicolet iN10MX) was performed with a liquid-nitrogen-cooled mercury cadmium telluride detector and an objective lens (15 ×). Regarding Kirchhoff's law of thermal radiation, the emissivity was equal to the absorptivity. Here, transmissivity was neglected because of the thick bottom layer. Thus, the reflectivity of the sample was measured by exposing the metasurface to a Globar beam with the same beam size as that in microspectroscopy with the spectral

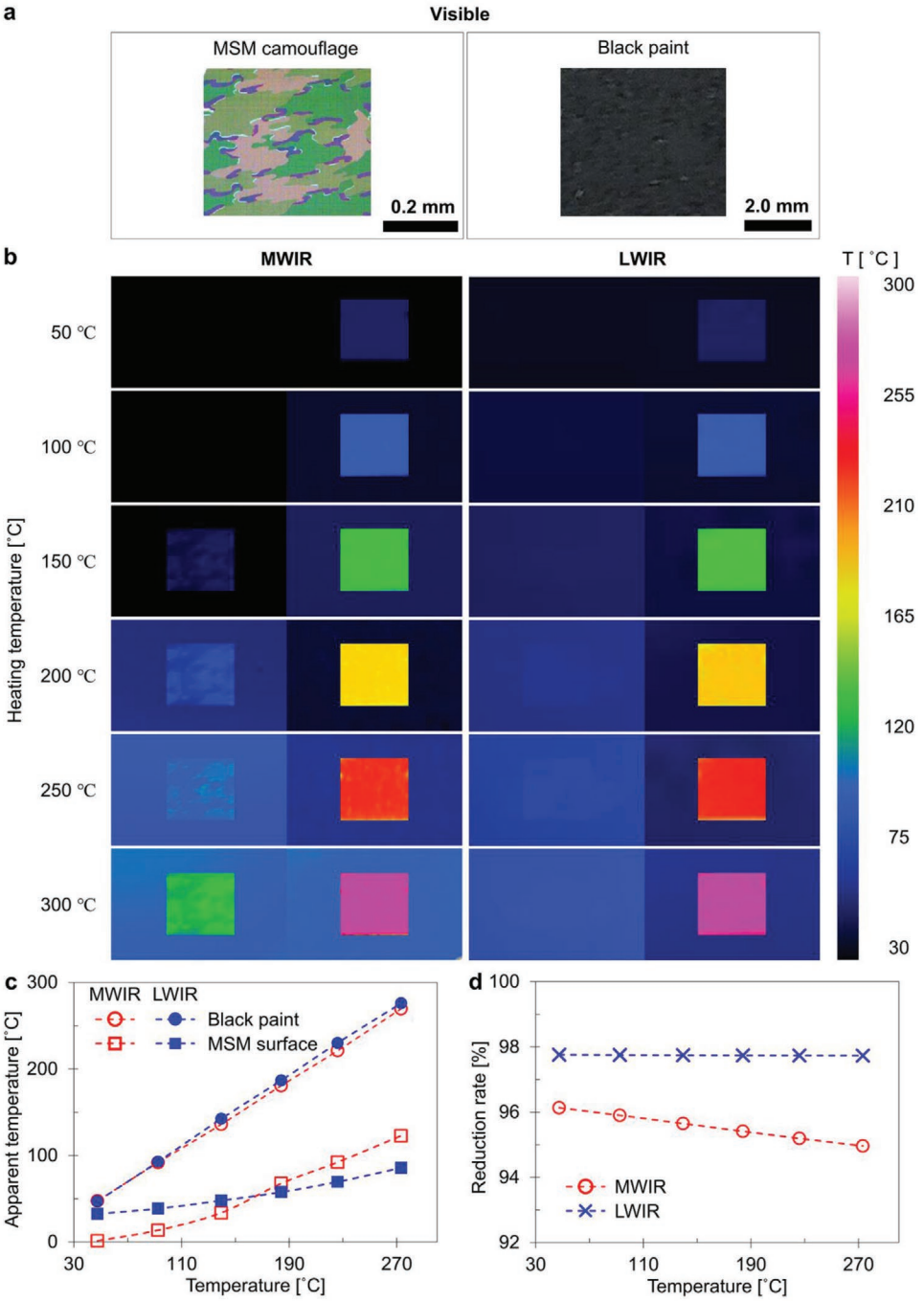

Figure 4. Visible and IR images of square printed with the MSM metasurface and black paint. a) Optical microscopy images. b) IR images recorded by the MWIR and LWIR cameras, listed in the left and right columns, respectively. c) Apparent temperatures measured with MWIR and LWIR cameras. d) Estimated reduction rate of the IR signature with temperature change.

resolution of 1 cm^{-1}. Moreover, a silver-coated mirror was used as a perfect reflector. The spectral reflected intensity of the silver mirror was recorded using FTIR spectroscopy and calibrated all the measurement data with the spectral reflectance of the silver film.

Measurement of Optical Images: Optical images of the metasurface were acquired via optical microscopy (Olympus, BX51M). Before obtaining the color images, the white point was set using the reference sample deposited with the silver material. The images were captured by illumination with a halogen light source. To obtain the IR images, MWIR (FLIR, SC5600, spectral response 3–5 µm) and LWIR cameras (Infratec, VarioCAM Hdx600) were used at the Daedeok Center of Korea Basic Science Institute (KBSI). Furthermore, a digital temperature controller (Global Lab, GLTC-DP) was used, which was connected to a heating tape to maintain the temperature of the sample at the set temperature, 50–300 °C.

Numerical Calculation: A commercial FDTD software (Lumerical) was adopted to calculate the spectral absorptivity of the MSM metasurface. A broadband plane wave in the TM mode was incident on a unit cell of an MSM metasurface that was subjected to periodic boundary conditions in the *xy* direction. A transmission monitor that detected the waves

reflected from the structure was positioned near the source at a distance of $\lambda/4$ from the structure to avoid interference from evanescent waves from the structure. To minimize the scattering error of the light incident on the upper boundary layer, a perfectly matched layer condition along the *z*-direction was used with the maximum number of systems, 64.

Supporting Information

Supporting Information is available from the Wiley Online Library or from the author.

Acknowledgements

This research was mainly supported by a National Research Foundation of Korea (NRF) grant funded by the Ministry of Science and ICT under project no. NRF-2020M3F6A1081011-1711119179. This research was also supported in part by the Ministry of SMEs and Startups (MSS, Korea under project no. 10437780).

Conflict of Interest

The authors declare no conflict of interest.

Author Contributions

J.K. and C.P. contributed equally to this work. J.W.H., J.K. and C.P. conceived the project. J.K. designed the structure, performed FDTD simulation, fabricated the devices and conducted experiment. C.P. performed theoretical analysis on F-P resonance. All authors co-wrote the manuscript, analyzed the data, and contributed to discussion.

Data Availability Statement

The data that supports the findings of this study are available in the supplementary material of this article.

Keywords

camouflage patterns, metal–semiconductor–metal metasurfaces, multiband infrared stealth technology, thermal and reflective signature reduction

Received: September 13, 2021
Revised: December 6, 2021
Published online: January 25, 2022

[1] S. A. Morin, F. Robert, S. W. Kwok, A. A. Stokes, A. Nemiroski, G. M. Whitesides, *Science* **2012**, *337*, 828.
[2] L. Phan, W. G. Walkup, D. D. Ordinario, E. Karshalev, J. M. Jocson, A. M. Burke, A. A. Gorodetsky, *Adv. Mater.* **2013**, *25*, 5621.
[3] J. Teyssier, S. V. Saenko, D. van der Marel, M. C. Milinkovitch, *Nat. Commun.* **2015**, *6*, 6368.
[4] G. Wang, X. Chen, S. Liu, C. Wong, S. Chu, *ACS Nano* **2016**, *10*, 1788.
[5] P. Won, K. K. Kim, H. Kim, J. J. Park, I. Ha, J. Shin, J. Jung, H. Cho, J. Kwon, H. Lee, S. H. Ko, *Adv. Mater.* **2021**, *33*, 2002397.
[6] J. V. Ramana Rao, D. S. Bedi, *Introduction to Camouflage and Deception*, Defence Scientific Information & Documentation Centre (DESIDOC), DRDO Monographs/Special Publications Series, New Delhi **1999**.
[7] J. Kim, K. Han, J. W. Hahn, *Sci. Rep.* **2017**, *7*, 6740.
[8] O. Salihoglu, H. B. Uzlu, O. Yakar, S. Aas, O. Balci, N. Kakenov, S. Balci, S. Olcum, S. Süzer, C. Kocabas, *Nano Lett.* **2018**, *18*, 4541.
[9] R. Hu, S. Zhou, Y. Li, D.-Y. Lei, X. Luo, C.-W. Qiu, *Adv. Mater.* **2018**, *30*, 1707237.
[10] R. Hu, S. Huang, M. Wang, X. Luo, J. Shiomi, C.-W. Qiu, *Adv. Mater.* **2019**, *31*, 1807849.
[11] H. Zhu, Q. Li, C. Zheng, Y. Hong, Z. Xu, H. Wang, W. Shen, S. Kaur, P. Ghosh, M. Qiu, *Light: Sci. Appl.* **2020**, *9*, 60.
[12] C. Park, J. Kim, J. W. Hahn, *ACS Appl. Mater. Interfaces* **2020**, *12*, 43090.
[13] Y. Liu, J. Song, W. Zhao, X. Ren, Q. Cheng, X. Luo, N. X. Fang, R. Hu, *Nanophotonics* **2020**, *9*, 855.
[14] R. Hu, W. Xi, Y. Liu, K. Tang, J. Song, X. Luo, J. Wu, C.-W. Qiu, *Mater. Today* **2021**, *45*, 120.
[15] J. Zhang, S. Huang, R. Hu, *Chin. Phys. Lett.* **2021**, *38*, 010502.
[16] J. Battaglia, R. Brubaker, M. Ettenberg, D. Malchow, *Proceedings of SPIE* **2007**, *6541*, 654106.
[17] M. Pan, Y. Huang, Q. Li, H. Luo, H. Zhu, S. Kaur, M. Qiu, *Nano Energy* **2020**, *69*, 104449.
[18] J. Lee, H. Sul, Y. Jung, H. Kim, S. Han, J. Choi, J. Shin, D. Kim, J. Jung, S. Hong, S. H. Ko, *Adv. Funct. Mater.* **2020**, *30*, 2003328.
[19] C. Park, J. Kim, J. W. Hahn, *Adv. Opt. Mater.* **2021**, https://doi.org/10.1002/adom.202002225.
[20] H. Zhu, Q. Li, C. Tao, Y. Hong, Z. Xu, W. Shen, S. Kaur, P. Ghosh, M. Qiu, *Nat. Commun.* **2021**, *12*, 1805.
[21] Y. Qu, Q. Li, K. Du, L. Cai, J. Lu, M. Qiu, *Laser Photonics Rev.* **2017**, *11*, 1700091.
[22] J. Hao, J. Wang, X. Liu, W. J. Padilla, L. Zhou, M. Qiu, *Appl. Phys. Lett.* **2010**, *96*, 251104.
[23] N. Liu, M. Mesch, T. Weiss, M. Hentschel, H. Giessen, *Nano Lett.* **2010**, *10*, 2342.
[24] A. Moreau, C. Ciraci, J. J. Mock, R. T. Hill, Q. Wang, B. J. Wiley, A. Chilkoti, D. R. Smith, *Nature* **2012**, *492*, 86.
[25] M. Yan, *J. Opt.* **2013**, *15*, 025006.
[26] D. Zhao, L. Meng, H. Gong, X. Chen, Y. Chen, M. Yan, Q. Li, M. Qiu, *Appl. Phys. Lett.* **2014**, *104*, 221107.
[27] J. Song, S. Huang, Y. Ma, Q. Cheng, R. Hu, X. Luo, *Opt. Express* **2020**, *28*, 875.
[28] W. L. Barnes, A. Dereux, T. W. Ebbesen, *Nature* **2003**, *424*, 824.
[29] A. Pors, M. G. Nielsen, T. Bernardin, J.-C. Weeber, S. I. Bozhevolnyi, *Light: Sci. Appl.* **2014**, *3*, e197.
[30] T. D. Dao, K. Chen, S. Ishii, A. Ohi, T. Nabatame, M. Kitajima, T. Nagao, *ACS Photonics* **2015**, *2*, 964.
[31] X. Zhu, C. Vannahme, E. Højlund-Nielsen, N. A. Mortensen, A. Kristensen, *Nat. Nanotechnol.* **2016**, *11*, 325.
[32] S. Wang, P. C. Wu, V. C. Su, Y. C. Lai, C. H. Chu, J. W. Chen, S. H. Lu, J. Chen, B. Xu, C. H. Kuan, T. Li, S. Zhu, D. P. Tsai, *Nat. Commun.* **2017**, *8*, 187.
[33] K. Kumar, H. Duan, R. S. Hegde, S. C. W. Koh, J. N. Wei, J. K. W. Yang, *Nat. Nanotechnol.* **2012**, *7*, 557.
[34] M. A. Kats, A. Blanchard, P. Genevet, F. Capasso, *Nat. Mater.* **2013**, *12*, 20.
[35] Z. Li, S. Butun, K. Aydin, *ACS Photonics* **2015**, *2*, 183.
[36] K.-T. Lee, J.-Y. Jang, S. J. Park, C. Ji, S.-M. Yang, L. J. Guo, H. J. Park, *Adv. Opt. Mater.* **2016**, *4*, 1696.
[37] H. Wang, X. Wang, C. Yan, H. Zhao, J. Zhang, C. Santschi, O. J. F. Martin, *ACS Nano.* **2017**, *11*, 4419.
[38] X. Duan, S. Kamin, N. Liu, *Nat. Commun.* **2017**, *8*, 14606.

[39] X. Zhu, W. Yan, U. Levy, N. A. Mortensen, A. Kristensen, *Sci. Adv.* **2017**, *3*, e1602487.
[40] W. Yang, S. Xiao, Q. Song, Y. Liu, Y. Wu, S. Wang, J. Yu, J. Han, D. P. Tsai, *Nat. Commun.* **2020**, *11*, 1864.
[41] Z. Li, P. Lin, Y. W. Huang, J. S. Park, W. T. Chen, Z. Shi, C. W. Qiu, J. X. Cheng, F. Capasso, *Sci. Adv.* **2021**, *7*, eabe4458.
[42] A. Ciesielski, L. Skowronski, W. Pacuski, T. Szoplik, *Mater. Sci. Semicond. Process.* **2018**, *81*, 64.
[43] T. Amotchkina, M. Trubetskov, D. Hahner, V. Pervak, *Appl. Opt.* **2020**, *59*, A40.
[44] E. D. Palik, *Handbook of Optical Constants of Solids*, 1st Ed., Vol. *2*, Academic Press, San Diego, CA, **1991**.
[45] H.-J. Hagemann, W. Gudat, C. Kunz, *J. Opt. Soc. Am.* **1975**, *65*, 742.
[46] J. Shin, J. Ko, S. Jeong, P. Won, Y. Lee, J. Kim, S. Hong, N. L. Jeon, S. H. Ko, *Nat. Mater.* **2021**, *20*, 100.